

Comparison of x-ray absorption spectra between water and ice: New ice data with low pre-edge absorption cross-section

Jonas A. Sellberg, Sarp Kaya, Vegard H. Segtnan, Chen Chen, Tolek Tyliczszak, Hirohito Ogasawara, Dennis Nordlund, Lars G. M. Pettersson, and Anders Nilsson

Citation: *The Journal of Chemical Physics* **141**, 034507 (2014); doi: 10.1063/1.4890035

View online: <http://dx.doi.org/10.1063/1.4890035>

View Table of Contents: <http://scitation.aip.org/content/aip/journal/jcp/141/3?ver=pdfcov>

Published by the [AIP Publishing](#)

Articles you may be interested in

[Cross-nucleation between clathrate hydrate polymorphs: Assessing the role of stability, growth rate, and structure matching](#)

J. Chem. Phys. **140**, 084506 (2014); 10.1063/1.4866143

[Molecular simulation of the crystallization of aluminum from the supercooled liquid](#)

J. Chem. Phys. **127**, 144509 (2007); 10.1063/1.2784120

[SpinSensitive and Angular Dependent Detection of Resonant Excitations at the K Absorption PreEdge of \$\alpha\$ Fe₂O₃](#)


AIP Conf. Proc. **882**, 861 (2007); 10.1063/1.2644685

[Unified interpretation of preedge xray absorption fine structures in 3d transition metal compounds](#)

AIP Conf. Proc. **652**, 497 (2003); 10.1063/1.1536411




[Atomic form factors and photoelectric absorption crosssections near absorption edges in the soft Xray region](#)

AIP Conf. Proc. **652**, 370 (2003); 10.1063/1.1536398



AIP | The Journal of
Chemical Physics

Meet The New Deputy Editors

	Peter Hamm		David E. Manolopoulos		James L. Skinner
---	-------------------	---	------------------------------	---	-------------------------

Comparison of x-ray absorption spectra between water and ice: New ice data with low pre-edge absorption cross-section

Jonas A. Sellberg,^{1,2} Sarp Kaya,² Vegard H. Segtnan,^{2,3} Chen Chen,^{2,4} Tolek Tyliczszak,⁵ Hirohito Ogasawara,⁶ Dennis Nordlund,⁶ Lars G. M. Pettersson,¹ and Anders Nilsson^{1,2}

¹Department of Physics, AlbaNova University Center, Stockholm University, S-106 91 Stockholm, Sweden

²SUNCAT Center for Interface Science and Catalysis, SLAC National Accelerator Laboratory, 2575 Sand Hill Road, Menlo Park, California 94025, USA

³Nofima AS, N-1430 Ås, Norway

⁴Department of Chemistry, Stanford University, Stanford, California 94305, USA

⁵Advanced Light Source, Lawrence Berkeley National Laboratory, Berkeley, California 94720, USA

⁶Stanford Synchrotron Radiation Lightsource, SLAC National Accelerator Laboratory, P.O. Box 20450, Stanford, California 94309, USA

(Received 26 March 2014; accepted 1 July 2014; published online 21 July 2014)

The effect of crystal growth conditions on the O K-edge x-ray absorption spectra of ice is investigated through detailed analysis of the spectral features. The amount of ice defects is found to be minimized on hydrophobic surfaces, such as BaF₂(111), with low concentration of nucleation centers. This is manifested through a reduction of the absorption cross-section at 535 eV, which is associated with distorted hydrogen bonds. Furthermore, a connection is made between the observed increase in spectral intensity between 544 and 548 eV and high-symmetry points in the electronic band structure, suggesting a more extended hydrogen-bond network as compared to ices prepared differently. The spectral differences for various ice preparations are compared to the temperature dependence of spectra of liquid water upon supercooling. A double-peak feature in the absorption cross-section between 540 and 543 eV is identified as a characteristic of the crystalline phase. The connection to the interpretation of the liquid phase O K-edge x-ray absorption spectrum is extensively discussed.
 © 2014 AIP Publishing LLC. [<http://dx.doi.org/10.1063/1.4890035>]

I. INTRODUCTION

O K-edge x-ray absorption features measured through either x-ray absorption spectroscopy (XAS) or hard x-ray Raman scattering (XRS) have become standard techniques to elucidate the hydrogen (H-) bonding structure in liquid water, ices, aqueous solutions, and water at interfaces.^{1–39} In XAS the photon energy is scanned to resonantly excite an O 1s electron while in XRS the energy-loss of high-energy photons is measured, which, in the small momentum transfer limit, becomes almost identical to XAS. However, there has been an intense debate on how to interpret the XAS/XRS data of water and ice after the publication of the study of Wernet *et al.*³³ which concluded that most molecules in ambient water are in very asymmetric H-bonding configurations denoted single-donor (SD) species rather than maintaining four H-bonds as in the traditional tetrahedral picture. Based on other x-ray spectroscopic and scattering results^{9,17,40–43} and recently also vibrational spectroscopy data⁴⁴ a hypothesis has been proposed that the water structure can be described in terms of fluctuations between two classes of local structures. At ambient temperature most molecules favor a closer packing than tetrahedral, with strongly distorted H-bonds. This allows the quantized librational modes to be excited and contribute to the entropy, but with enthalpically favored, tetrahedrally bonded water patches appearing as fluctuations, i.e., a competition between entropy and enthalpy.¹⁷

This hypothesis is under heated debate^{17,45–51} but can be directly related to observations of supercooled water where

fluctuations increase anomalously and thus be connected with the much debated existence of a liquid-liquid transition and critical point between a high-density (HDL) and low-density (LDL) liquid.^{52,53} The HDL phase would be related to the disordered asymmetric species observed through XAS and the LDL to the tetrahedral patches in the fluctuations around equilibrium at a given temperature. HDL maximizes the entropy while LDL minimizes the enthalpy; these are key quantities for the interaction of water with a hydrophobic solute, biomolecule, or membrane.

XAS probes the unoccupied molecular orbitals of a system through the excitation of a core electron. In particular, it can be shown that the pre- (535 eV) and main-edge peaks (537–538 eV) fingerprint distorted H-bonds, whereas the post-edge (540–542 eV) is associated with strong H-bonds and is further enhanced for tetrahedrally H-bonded structures.^{15,54} In the x-ray absorption spectrum of liquid water, excitation into localized,⁵⁵ low-lying orbitals gives rise to the pre- and main-edge features that are signatures of weak or distorted H-bonds in water.^{7,12,15,33} The post-edge peak, on the other hand, is due to excitation into delocalized states in the conduction band⁵⁵ and gains intensity from intact or strong H-bonds.^{7,12,15} The main-edge feature, at around 537 eV is enhanced upon formation of high-density amorphous ice²⁸ and various crystalline high-pressure ice phases, such as I_{II}, I_{VI}, I_{VII}, and I_{VIII}.¹⁹ This enhancement is related to the fact that the second shell collapses from the tetrahedral distance of 4.52 Å in hexagonal ice to much shorter

distances leading to an overall higher density. As a consequence, H-bonds become less directional which allows post-edge intensity to move into the main-edge region. It is clearly established that in water the pre-edge and main-edge features increase while the post-edge decreases in intensity with increasing temperature with the appearance of an isosbestic point.^{15,20,33}

It is essential that we can bring further information regarding this interpretation of XAS/XRS of H-bonded systems, such as water. In particular since there is a lack of agreement on the quality of various theoretical approaches to compute the x-ray absorption spectrum of water. The transition-potential, half core hole (HCH) approach of Triguero *et al.*⁵⁶ has been successfully applied to a large number of systems.^{57–61} Using this approach, ice-like spectra are obtained from simulated water, except when selecting molecules with significantly enhanced H-bond asymmetry.⁶² Calculations using a full core hole with screening from including the excited electron at the bottom of the conduction band (XCH)⁶³ reproduced some but not all features based on structures from a simulation of TIP4P water. Using a full, unscreened core hole Car and coworkers⁶⁴ computed spectra of both ice and liquid, but it was later shown that the full core hole (FCH) potential leads to too much intensity in the low-energy region of the spectrum.⁶⁵ Turning instead to the Bethe-Salpeter formalism with static Coulomb hole and screened exchange (COHSEX) led to strongly improved results, but still with significant deviations from experiment.⁶⁶ Taking nuclear quantum effects into account in the simulated structures led to further improvements, but with some discrepancies remaining.⁶⁷ A similar development using the Bethe-Salpeter formalism has been made by the group of Rehr.⁶⁸ In all these efforts it is unclear whether the difficulties lie mainly in the strength of the core-hole potential or in the underlying structures from molecular dynamics (MD).

The water spectrum has now been established to very high accuracy.¹⁵ However, the details of the spectra of hexagonal (I_h) and cubic (I_c) ice remain less clear experimentally. Since there is a debate regarding the structure of the liquid, ice I_h , for which the structure is well-known, has become the prototype to benchmark theoretical calculations to describe the x-ray absorption process.^{57,63,66–69} Is there a pre-edge feature inherent in hexagonal ice? Based on symmetry arguments of the tetrahedral arrangement in ice and the dipole selection rule it was proposed that there should only be some faint pre-edge intensity due to vibronic coupling, similar to what is observed for the lowest excited state in methane.¹⁵ Most experimental ice spectra, however, do show a pre-edge peak^{15,19,20,28} whereas two-dimensional H-bonded adsorbed ice films on metal surfaces,⁵⁴ measured with the electric field vector parallel to the surface, indicate only a very weak pre-edge as expected from the symmetry argument.¹⁵ Some studies claim that there is only a small difference in pre-edge intensity between water and ice and that the pre-edge feature is inherent to the ice spectrum.^{20,28} However, these studies used XRS and, even though small momentum transfer was utilized, contributions from non-dipole transitions are difficult to eliminate.¹⁵ Recently, using resonant inelastic x-ray scattering (RIXS) with vibrational resolution it was shown that

molecular species giving rise to the pre-edge intensity in water are connected to the blueshifted part of the OH-stretch vibrational spectrum indicative of broken or strongly weakened H-bonds.⁷⁰ It has furthermore been shown that the intensity of the pre-edge in ice spectra depends on the procedure used to prepare the samples.¹⁵ Another question is whether we, based on the difference between ice and water spectra, can view the water spectrum as originating from two different spectral moieties in terms of local HDL and LDL structures.

In this study we present new spectra of both crystalline ice and water in order to provide deeper insights into some of these questions. We have prepared ice samples using two different procedures and measured spectra using XAS where no non-dipole transition can contribute to the pre-edge intensity. The first sample was obtained by freezing a thin film of liquid water and measuring the x-ray absorption spectrum in transmission mode with the sample kept at a relatively high temperature. The other sample is a film of ice crystallites on a BaF_2 surface prepared under crystalline ice-growth conditions in ultra-high vacuum. The substrate is a freshly cleaved crystal that will have few nucleation sites on the surface which favors growth of larger crystallites. This reduces the influence of grain boundaries and leads to an ice sample which we anticipate contains fewer defects. We have also conducted temperature-dependence measurements of water using transmission XAS instead of XRS so a more careful comparison can be made of the changes in the spectra upon supercooling the liquid and upon ice crystallization. These results will be put into the context of our understanding of XAS of water and ice and how it relates to the overall picture of the structure of liquid water.

II. METHODS

A. Experimental setup at BL11.0.2, Advanced Light Source (ALS)

XAS transmission measurements were performed at the Scanning Transmission X-ray Microscopy (STXM) end-station⁷¹ at beam line (BL) 11.0.2 at the ALS. Deionized water (PURELAB Ultra Genetic or Millipore, resistivity 18.2 M Ω cm at 298 K) was injected into a sample cell (described in detail in Ref. 30) with 200 nm thick Si_3N_4 windows. The sample cell was cooled by a 1.5 W Peltier element (TEC 00711-5L31-03CA from Custom Thermoelectric) attached to a custom-made Cu sample holder, which in turn was cooled through Cu foil by a liquid N_2 reservoir. The temperature was controlled by adjusting the Peltier output power and the He pressure in the chamber (700 Torr at 299 K, 2×10^{-5} Torr at 232 K), and was measured through a K-type (chromel-alumel) thermocouple connected to the outside of the sample cell. The photon energy of the synchrotron beam was selected by a planar grating monochromator with an energy resolution of 0.1–0.2 eV, and was scanned between 525 and 560 eV. Measurement scans were performed with 0.05–0.204 eV steps (0.1–0.667 eV steps above 544 eV) and 5 ms dwell time per step; the sample was moved 0.1 μm between each step to minimize beam-induced damage. The temperature was controlled to ± 1 K or better during spectrum acquisition,

which is comparable to the absolute temperature accuracy of ± 1.5 K for K-type thermocouples (IEC 584-2 standard). The cooling rate at which the ice was formed was approximately 1 K/min.

The intensity of the transmitted beam was measured using a photomultiplier tube (PMT) behind the sample for both an empty (I_0) and filled cell (I), from which the absorbance A can be obtained as a function of photon energy through the Beer-Lambert law, $I = I_0 \exp(-A) = I_0 \exp(-n\sigma_{\text{tot}}z)$, where z is the sample thickness (m), n is the number density (molecules/m³), and σ_{tot} is the total cross-section (m²/molecule). As the transmitted intensity depends exponentially on the sample thickness, the incident beam was focused with a 45 nm Fresnel zone plate to ~ 50 nm—resulting in I_0 of about 1.5×10^6 photons/s or a flux of 760 photons/nm² s—to make sure the illuminated volume had a uniform sample thickness. Sample areas with absorbance differences of less than 10% were averaged to increase statistics. The photon energy was calibrated against the pre-edge peak in the x-ray absorption spectrum of water (H₂O) at 298 K, which has been determined previously to be positioned at 535.0 eV.¹⁴

B. Experimental setup at BL13-2, Stanford Synchrotron Radiation Lightsource (SSRL)

XAS secondary electron yield (SEY) measurements were carried out at the Surface Science Endstation (SSE) at the elliptical undulator beam line 13-2 at SSRL. The BaF₂ crystal was freshly cleaved along the (111) plane prior to sample loading without prolonged exposure to air. The Mo sample holder was transferred to the ultra-high vacuum (UHV) chamber through a load lock system. A W filament was used to heat up the sample and desorb any adsorbates while liquid N₂ cooled the sample holder; the temperature at the sample was probed by a K-type (chromel-alumel) thermocouple. The base pressure of the UHV chamber was 2×10^{-10} Torr at 200 K. A pulsed gas delivery system was used to dose 360×5 ms-pulses of D₂O—corresponding to 30 monolayers (ML)—onto the clean BaF₂(111) surface while annealed to 144 K for 18 min. A monolayer is assumed to be equivalent to the amount of a single layer of water on Ni(111) as calibrated by XPS when using the same dosing procedure at 100 K without annealing.¹⁵

X-ray absorption spectra were recorded at 95 K at a grazing angle of 2–3° by monitoring the secondary electrons with kinetic energy of 12 eV and pass energy of 200 eV using a VG-Scienta R3000 hemispherical electron spectrometer. The synchrotron beam—with the polarization set to be parallel to the (111) surface—was focused to $8 \times 50 \mu\text{m}^2$ on the sample at I_0 of about 4.4×10^{10} photons/s, corresponding to a flux of 110 photons/nm² s. The photon energy of the synchrotron beam was selected by a spherical grating monochromator with an energy resolution of 0.12 eV, and was scanned between 520 and 560 eV. Measurement scans were performed with 0.1 eV steps (0.25 eV steps above 550 eV) and 1–2 s dwell time per step. The photon energy was calibrated by measuring the difference in kinetic energy of photoelectrons emitted from the Fermi level of the Mo sample holder

using 1st and 2nd order light at 525 eV and the energy dispersion was measured by taking the kinetic energy difference of emitted electrons at 525 and 560 eV photon energies. The accuracy of the determination of the Fermi level at 2nd order was estimated to be approximately ± 0.05 eV; the non-linearity of the electron spectrometer is expected to be smaller than ± 0.1 eV.

For thin samples or surface-sensitive detection techniques, the photon intensity throughout the sample can be considered constant and it is possible to Taylor expand the transmitted intensity around $A = 0$. This yields that the intensity of the secondary electrons, I_{SEY} , which is proportional to the absorbed photon intensity, depends linearly on the absorbance: $I_{\text{SEY}} = I_0 (1 - \exp(-A)) = I_0 (1 - 1 + A + \dots) \approx I_0 A = I_0 n\sigma_{\text{tot}}z$. The spectra were then normalized to the incoming photon flux I_0 , and the background from the substrate was subtracted. To compare the two isotopes, the D₂O spectra were shifted by -0.16 eV, corresponding to the difference in zero-point energy (ΔZPE) between D₂O and H₂O.¹⁵

C. Data analysis

The total cross-section σ_{tot} was derived from the absorbance by area-normalizing over the whole O K-edge (532.5–550 eV), thus removing any contribution from the sample thickness or number density. The scattering contribution to σ_{tot} is assumed to be constant over the scanned energy range and is removed through a constant background subtraction, leaving the residual absorption cross-section σ_{A} . Differences in absorption cross-section between ice and liquid, as well as between liquid samples at different temperatures, were calculated by subtracting the absorption cross-section of the STXM transmission spectrum of bulk H₂O (l) measured at 299 K. To compute the difference spectra, an interpolation of the data was made between 530 and 560 eV with 0.05 eV steps.

The 2nd derivative (with respect to photon energy E) of $\sigma_{\text{A}}(E)$ was calculated using a Savitzky-Golay smoothing filter of 2nd order,⁷² which is a local polynomial regression of degree 2 using a 31-point window size, corresponding to 1.50 eV. The coefficient of the quadratic term in the polynomial then determines the 2nd derivative. The Savitzky-Golay smoothing filter reduces the level of noise in the spectra, but may introduce smoothing errors. To estimate the error bars of the smoothed spectra, the standard deviation of the difference between the raw data and the smoothed data was computed for the local 31-point window, resulting in error curves that cover a 95.4% confidence interval (two standard deviations).

Principal component analysis,^{73–76} which is an orthogonal linear transformation of the original data, was used to reduce the number of dimensions of the spectral matrix similar to previous studies using infrared spectroscopy,^{77,78} XAS,⁷⁹ and nuclear magnetic resonance spectroscopy.⁸⁰ Principal component analysis was performed by mean-centering the spectral ensemble, after which the covariance matrix was calculated and diagonalized. The eigenvectors of the covariance matrix were ordered after decreasing magnitude of their corresponding eigenvalues, where the 1st principal

component is the eigenvector/eigenvalue pair with largest explained variance. We name the eigenvectors the loadings of the principal components and their scores associated with each spectrum (i.e., the representations of the spectra in the principal component space) are calculated by multiplying the loadings with the mean-centered spectral matrix. The spectra were smoothed using a Savitzky-Golay filter,⁷² as described above, prior to calculating the principal components. The score of the 1st principal component was used to model the temperature-dependence of the water spectra by linear regression (i.e., principal component regression using a one-component model). Full cross-validation of the spectral ensemble was utilized to calculate the predicted temperatures. Note that the smoothing was only applied for the principal component analysis and for finding second derivatives as described above.

III. RESULTS

In order to understand the spectral features of ice in detail, we first report the temperature-dependent changes of liquid water including the well-established water spectrum at room temperature.

The O K-edge x-ray absorption spectra of water at four different temperatures are shown in Fig. 1. All spectra show three absorption features: a well-resolved pre-edge peak at 535 eV, a main-edge at 537–538 eV, and a post-edge shoulder centered around 541 eV. The spectrum at 299 K is in agreement with the typical absorption cross-section of water at room temperature measured in previous studies using XAS^{15,33} as well as XRS.^{9,15,20,33} Upon cooling the liquid the absorption cross-section is reduced at the pre-edge and main-edge, whereas the post-edge shoulder becomes more prominent. These changes are enhanced in the top section of Fig. 1, where the differences in absorption cross-section relative to water at 299 K are shown. Note that there appears to be an isosbestic point at 539.7 eV. These results are fully consistent with previous temperature-dependent XRS data,^{9,15,20,33} but here reported at the higher resolution possible with XAS using soft x-rays and also without contribution from non-dipole intensity as well as extending the temperature range to the slightly supercooled regime. Spectra in the supercooled regime down to 254 K have been reported previously in the XAS study by Smith *et al.*,²⁷ but the spectra were strongly affected by saturation effects giving an incorrect relative temperature change between the main-edge and post-edge in comparison to the present study and previous XRS data.^{9,15,20,33}

Water deposited on a surface at temperatures lower than the glass transition temperature T_g (of low-density amorphous ice⁸¹) at 136 ± 2 K^{82–84} generally forms an amorphous layer of ice.⁸⁵ Annealing of this amorphous layer above T_g leads to crystallization and water desorption.^{85–90} The O K-edge x-ray absorption spectra of ice samples prepared in various ways are shown in Fig. 2. The Auger electron yield (AEY) spectrum of amorphous ice grown on Pt(111) (dashed blue line) shows the same spectral features as liquid water in Fig. 1, although the main-edge has shifted down to 537 eV and has become much sharper and the pre-edge and post-edge have, respec-

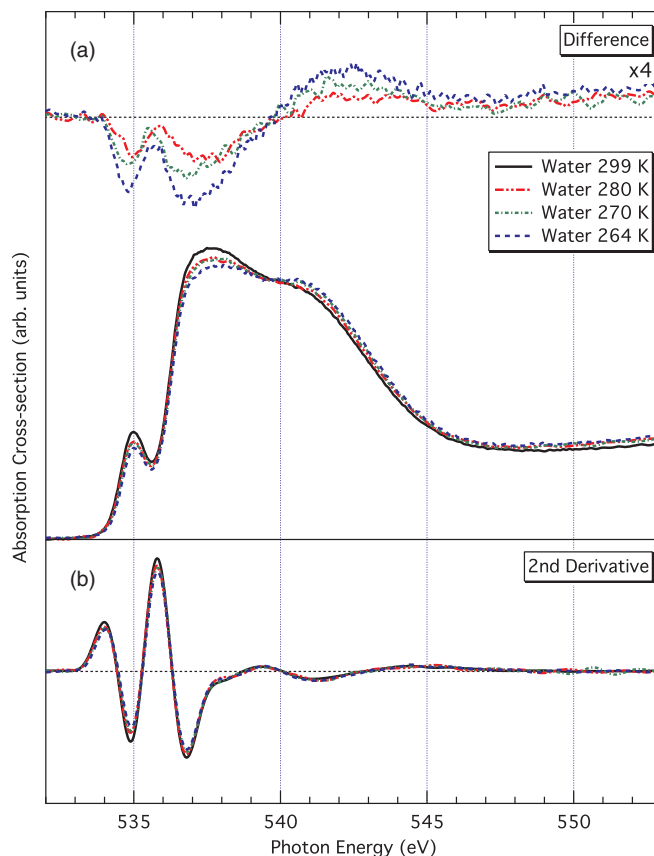


FIG. 1. (a) O K-edge x-ray absorption spectra of liquid water as a function of temperature (raw data). STXM transmission spectra of bulk water measured at 299 K (solid black curve), 280 K (double-dotted red curve), 270 K (single-dotted green curve), and 264 K (dashed blue curve) of 500–700 nm thick H_2O samples contained between Si_3N_4 windows. All spectra were background subtracted and area normalized between 532.5 and 550 eV. The top section shows the difference in absorption cross-section compared to the STXM transmission spectrum of bulk H_2O (l) measured at 299 K. The difference in absorption cross-section was magnified by a factor of 4 to highlight the spectral changes; the dotted black line denotes no difference. (b) 2nd derivatives of O K-edge x-ray absorption spectra of liquid water with identical markers and colors as in (a). Data were smoothed as described in Sec. II C. Positive peaks in the original intensity spectra are visible as negative minima in the 2nd derivatives of the intensity spectra. The black dashed line denotes zero in the 2nd derivative, corresponding to inflection points in the absorption cross-section.

tively, decreased and increased in absorption cross-section. The changes in the latter two are expected from extrapolation of the temperature-dependent changes in liquid water to 100 K, but the changes in the main-edge cannot be predicted by a linear extrapolation of the liquid water spectra (this is highlighted in Fig. 3(a), where the changes compared to water at 299 K are scaled to overlap in the pre-edge region). When the amorphous ice film grown on Pt(111) is annealed to 150 K (single-dotted green line) causing simultaneous crystallization and water desorption,^{86–90} the post-edge becomes sharper, stronger, and more structured; the pre-edge and main-edge also lose absorption cross-section but show similar changes (relative water at 299 K) as the amorphous ice spectrum. Crystalline ice films on Pt(111) prepared by isothermal heating of amorphous ice at 150 K have been suggested to consist of three-dimensional crystallites and be far from the intended homogeneous films, which is supported

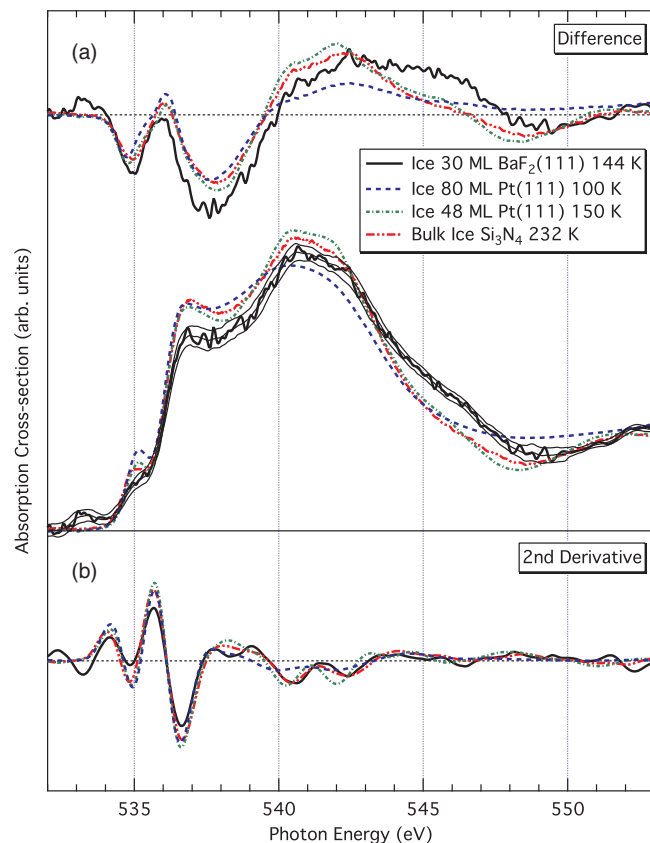


FIG. 2. (a) O K-edge x-ray absorption spectra of ice prepared under various growth conditions (raw data). SEY spectrum of crystalline ice prepared on BaF₂(111) (solid black curve) by depositing 30 ML of D₂O at 144 K; AEY spectrum of amorphous ice prepared on Pt(111) (dashed blue curve) by depositing 80 ML of D₂O at 100 K, an AEY spectrum of crystalline ice (single-dotted green curve) of 48 ML of D₂O was measured by annealing the amorphous film at 150 K and monitoring the desorption rate through mass spectrometry;¹⁵ STXM transmission spectrum of bulk crystalline ice (double-dotted red curve) at 232 K prepared by freezing an approximately 500 nm thick H₂O sample contained between Si₃N₄ windows. Due to the low signal-to-noise ratio in the raw data of the ice spectrum recorded on BaF₂(111), the smoothed spectrum ± 2 standard deviations (95.4% confidence interval) is shown as thin solid black lines. The D₂O spectra were shifted -0.16 eV to correct for the difference in zero-point energy between the two isotopes; the reference spectra on Pt(111)¹⁵ were shifted $+0.3$ eV to put all spectra on a common energy scale, as determined by the inflection point in the main-edge rise. All spectra were background subtracted and area normalized between 532.5 and 550 eV. The top section shows the difference in absorption cross-section compared to the STXM transmission spectrum of bulk H₂O (l) measured at 299 K; the dotted black line denotes no difference. (b) 2nd derivatives of O K-edge x-ray absorption spectra of ice with identical markers and colors as in (a). Data were smoothed as described in Sec. II C. Positive peaks in the original intensity spectra are visible as negative minima in the 2nd derivatives of the intensity spectra. The black dashed line denotes zero in the 2nd derivative, corresponding to inflection points in the absorption cross-section.

by x-ray photoelectron spectroscopy (XPS) and infrared reflection absorption spectroscopy (IRAS) that probe the intensity of the first monolayer compared to the total coverage.⁹¹ When bulk ice is prepared by freezing liquid water between Si₃N₄ membranes (double-dotted red line) and probed with STXM, a similar spectrum is obtained, indicating that the bulk ice formed is inhomogeneous in character with significant contributions from defects and grain boundaries. Nevertheless, these spectra are in agreement with previous crystalline ice studies using XAS³⁹ and XRS.¹⁹

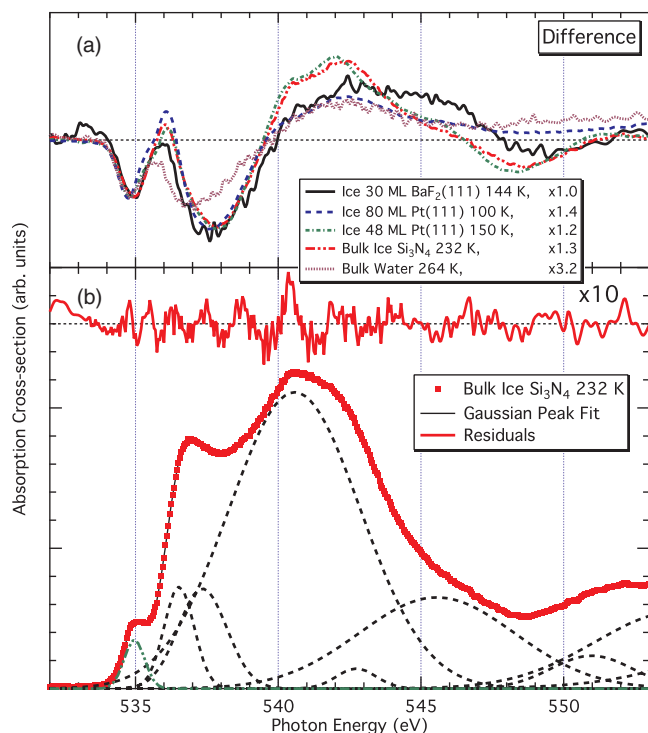


FIG. 3. Detailed analysis of the pre-edge spectral feature in the O K-edge x-ray absorption spectra (raw data). (a) Difference in absorption cross-section compared to the STXM transmission spectrum of bulk H₂O (l) measured at 299 K for the ice spectra shown in Fig. 2 (same color coding) and bulk H₂O (l) measured at 264 K (dotted purple curve). The difference spectra are scaled so that the change in the pre-edge overlaps; the scaling factor for each spectrum is given in the legend. The vertical dotted black line denotes no difference. (b) Gaussian peak fit analysis of STXM transmission spectrum of bulk crystalline ice (solid black curve) at 232 K prepared by freezing an approximately 500 nm thick H₂O sample contained between Si₃N₄ windows. The spectrum is deconvolved into 9 Gaussian peaks (dashed black curves, the Gaussian peak corresponding to the pre-edge is highlighted as the green dashed-dotted curve). The red squares denote the experimental data points and the solid red curve denotes the residuals of the least-squares fit (enlarged by a factor of 10); the horizontal dotted black line denotes zero.

However, when an ice film is prepared on BaF₂(111) the SEY spectrum (solid black line) shows large differences from the other crystalline ices. The pre-edge has clearly diminished in intensity and sits on top of the tail from the main-edge, which in turn is less intense than in spectra of bulk ice grown on other substrates. The post-edge on the other hand has shifted to significantly higher energy, with an indication of a split into two components, and a strong shoulder between 544 and 548 eV has appeared. Such a shoulder has been present in previous ice data,^{15,39} but with a much lower intensity. We note a minor contribution from OH at 533 eV, well separated from the rest of the spectrum; on insulating substrates beam-induced decomposition of water is difficult to eliminate completely.¹¹

The spectral features are emphasized in the 2nd derivative of the absorption cross-section, which is shown for all water and ice samples in Figs. 1(b) and 2(b), respectively. A peak in the absorption cross-section is seen as a minimum in the 2nd derivative, but the 2nd derivative spectral features appear sharper since there the Gaussian and Lorentzian peak-shapes have reduced width. For the water samples three minima are

TABLE I. Gaussian least-squares peak fit of the pre-edge for the various water and ice spectra. The peak position, peak amplitude, full width at half maximum (FWHM) of the peak, and the integrated peak area (corresponding to amplitude \times FWHM/2 $\sqrt{\ln(2)/\pi}$) are reported for each spectrum. The uncertainties correspond to one standard deviation in the confidence interval for the fit coefficients; the uncertainty was propagated to the calculated peak area as the maximum/minimum values attainable from errors of one standard deviation in peak amplitude and FWHM.

Spectrum	Position (eV)	Amplitude (arb. units)	FWHM (eV)	Area (eV, arb. units)
H ₂ O/Si ₃ N ₄ 299 K	534.94 \pm 0.005	0.0327 \pm 0.0006	0.94 \pm 0.008	0.033 \pm 0.0008
H ₂ O/Si ₃ N ₄ 280 K	534.93 \pm 0.003	0.0288 \pm 0.0003	0.91 \pm 0.007	0.028 \pm 0.0005
H ₂ O/Si ₃ N ₄ 270 K	534.96 \pm 0.008	0.0282 \pm 0.0007	0.91 \pm 0.014	0.027 \pm 0.0011
H ₂ O/Si ₃ N ₄ 264 K	534.97 \pm 0.005	0.0264 \pm 0.0005	0.89 \pm 0.014	0.025 \pm 0.0009
H ₂ O/Si ₃ N ₄ 232 K	534.96 \pm 0.008	0.0174 \pm 0.0005	0.84 \pm 0.015	0.016 \pm 0.0007
D ₂ O/Pt(111) 100 K	535.08 \pm 0.006	0.0230 \pm 0.0005	0.80 \pm 0.010	0.020 \pm 0.0007
D ₂ O/Pt(111) 150 K	535.06 \pm 0.012	0.0196 \pm 0.0007	0.78 \pm 0.020	0.016 \pm 0.0010
D ₂ O/BaF ₂ (111) 144 K	535.05 \pm 0.032	0.0072 \pm 0.0007	0.74 \pm 0.088	0.006 \pm 0.0012

visible, again associated with the pre-edge, main-edge, and post-edge. For the crystalline ice samples, however, the minimum associated with the post-edge has split up into two distinct peaks between 540 and 543 eV. The split of the post-edge appears to be the most significant spectral feature in the O K-edge spectrum that characterizes crystalline ice.

To quantify the changes in absorption cross-section in the various spectral regions, a Gaussian peak fit analysis consisting of 9 Gaussian peaks (1 for the pre-edge, 2–3 for the main-edge, 2–3 for the post-edge, 2–3 for the continuum region) was performed on all spectra. The curve fitting for the STXM spectra of ice at 232 K is shown in Fig. 3(b) as an example. Such an analysis is not unique and the result depends on the number of parameters and the initial conditions, but the intensity of the pre-edge, which is fairly isolated from the rest of the spectral components, can be determined with some accuracy. In Table I the peak position, peak amplitude, full width at half maximum (FWHM), and integrated area of the Gaussian peak that represents the pre-edge are reported for each spectrum. The trends deduced from visual inspection of the spectra are confirmed, decreasing pre-edge amplitude with decreasing temperature as well as after crystallization. We see that the ice film prepared on the BaF₂(111) surface has a significantly smaller pre-edge than the other crystalline samples amounting to about 40% of the pre-edge absorption cross-section for the crystalline ice film on Pt(111) and the bulk ice between Si₃N₄ membranes. We also note that the integrated pre-edge peak area is larger by a factor 5.7 in water at 299 K in comparison to ice on BaF₂(111). The peak position and FWHM of the pre-edge differ slightly (-0.11 ± 0.02 and 0.13 ± 0.05 eV, respectively) when comparing H₂O with D₂O (Table I), which can be attributed to a small uncertainty in the Δ ZPE calibration and the fact that no broadening has been added to account for the narrower spatial extent of the ground state vibrational wave function of D₂O compared to H₂O that in turn results in narrower peaks upon vertical excitation.¹⁵

To further analyze the spectral changes in more detail, principal component analysis was performed on the water and ice spectra. To visualize the decomposition of the spectra into principal components, the steps described in Sec. II C are shown in Fig. 4 for the O K-edge x-ray absorption spectrum of H₂O recorded at 299 K. First, smoothing

was performed to reduce the effect of noise in the spectra after which the mean of the spectral ensemble was computed (Fig. 4(a)). The mean of the spectral ensemble was subtracted from each spectrum (Fig. 4(b)) and the covariance matrix of all mean-centered spectra were calculated and diagonalized, resulting in principal components that are made up of normalized, orthogonal loadings with associated scores for each spectrum, i.e., the scores represent the spectrum in the principal component space. If all principal components are included (note that the total number of components are equal to the number of independent variables, or, in this case, energy bins in the spectra), the mean-centered spectra will be perfectly represented, but the number of independent variables may be reduced by only including the principal components with greatest explained variance. In Fig. 4(b), the 1st principal component representation is shown for the STXM spectrum at 299 K, which is calculated by multiplying the loading of the 1st principal component by the score associated with the spectrum. The residuals with respect to the original mean-centered spectrum are shown in Fig. 4(c) and are found to be orders of magnitude smaller than the spectral variations. Thus, the principal component analysis has reduced each spectrum to a single variable, namely, the score of the 1st principal component.

The loadings of the 1st principal component are shown in Fig. 5. The set consisting of only water spectra (double-dotted red line) had a 1st principal component that made up 97% of the explained variance; the associated scores of each spectrum are presented in Table II. The maxima at 535 and 537 eV indicate, respectively, a growing pre-edge and main-edge with increasing temperature. The broad minimum at \sim 542 eV shows that the temperature dependence of the post-edge is anti-correlated with the change in the pre-edge and main-edge, i.e., has an increasing absorption cross-section with decreasing temperature. The inset in Fig. 5 shows the predicted temperatures of the water spectra calculated from a linear regression model of the 1st principal component; using only the 1st principal component explains 87% of the sample temperature variation, indicating that the spectral changes in liquid water as a function of temperature are, to first order, linear in the temperature regime studied.

The set consisting of ice and water spectra (black solid line) had a 1st principal component that explained 78% of

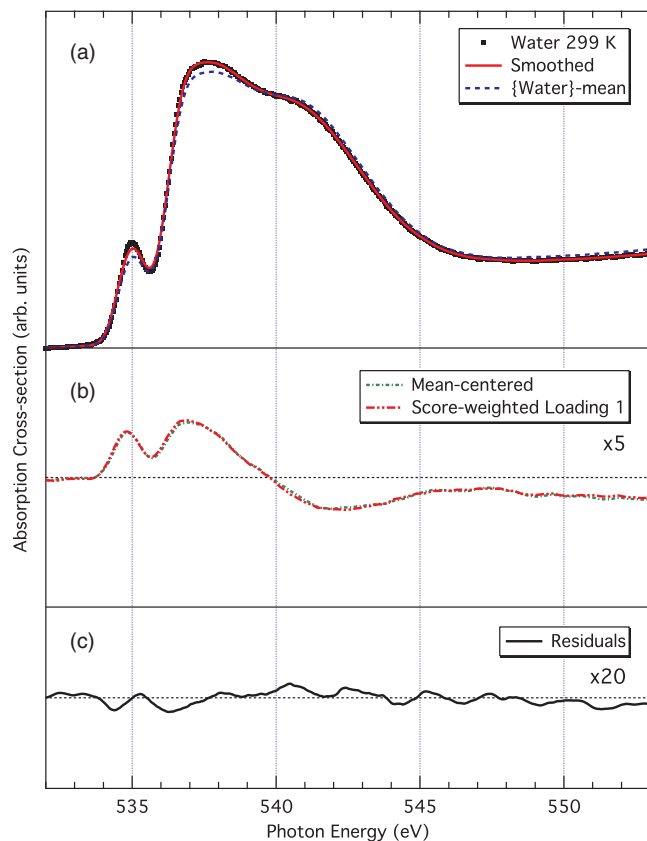


FIG. 4. Decomposition of the O K-edge x-ray absorption spectrum of bulk liquid water measured at 299 K into its 1st principal component. (a) STXM transmission spectrum of bulk water measured at 299 K; the black squares denote the experimental data points and the solid red curve denotes the smoothed data (details described in Sec. II C) used for principal component analysis. The STXM transmission spectrum at 299 K is compared to the mean (dashed blue curve) of the set consisting of all water spectra presented in Fig. 1 after smoothing. (b) Mean-centered spectrum at 299 K (single-dotted green curve) obtained after subtracting the mean of all water spectra (dashed blue curve) from the smoothed spectrum (red solid curve) in (a). The covariance matrix of all mean-centered spectra was calculated and diagonalized as described in Sec. II C, resulting in a 1st principal component that explains 97% of the variance in the spectral ensemble and whose representation of the mean-centered spectrum at 299 K (double-dotted red curve) can be obtained by scaling the loading shown in Fig. 5 with the score reported in Table II. Both the mean-centered spectrum and the 1st principal component representation were magnified by a factor of 5 compared to the spectra in (a). (c) The residuals of the 1st principal component representation at 299 K (solid black curve) with respect to the smoothed mean-centered spectrum shown in (b), enlarged by a factor of 20 compared to the spectra in (a).

the variance. The associated scores of each spectrum are presented in Table III and show positive scores between 0.08 and 0.14 for the water spectra, whereas the ice spectra have scores that span from -0.02 to -0.17 . It is evident that the 1st principal component can separate the crystalline ices (scores < -0.10) from the amorphous samples (scores > -0.05) as well as the liquids (scores > 0.05) from the solids (scores < 0.00). This clear separation between liquid samples, the amorphous ice, and the crystalline films are, for the former two, mainly related to the large temperature difference, but for the latter two attributed to phase and growth conditions. The maxima and minima of the loading of the 1st principal component were qualitatively similar to those of the water spectra, although several important quantitative differences can be

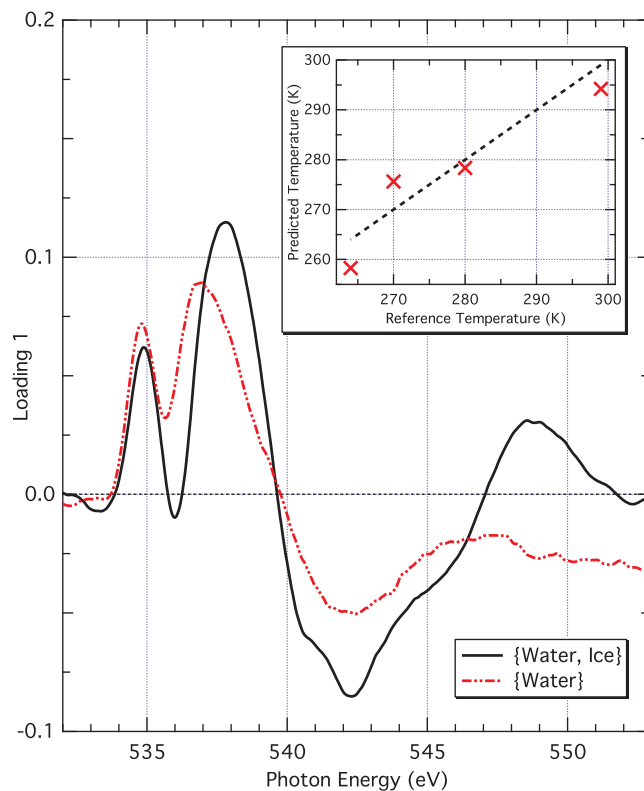


FIG. 5. Principal component analysis of O K-edge x-ray absorption spectra from Figs. 1 and 2. Data were smoothed as described in Sec. II C. The loading of the 1st principal component is shown as a function of photon energy for the set consisting of all water and ice spectra presented in Figs. 1 and 2 (solid black curve) and the set consisting of all water spectra presented in Fig. 1 (double-dotted red curve). The inset shows the predicted temperatures of the water spectra calculated from a linear regression model of the 1st principal component of the water ensemble (red crosses) plotted against the reference temperatures; the linear regression model of the 1st principal component had an R^2 value after full cross-validation of 0.872. The black dashed line indicates the targeted temperatures.

noted. The maximum associated with the main-edge is shifted to higher energies when the ice spectra are included and the minimum associated with the post-edge is sharper and much more structured than the diffuse peak observed for the set of water spectra. Furthermore, an additional maximum has developed at ~ 549 eV related to the minimum in absorption cross-section that is much more prominent for the crystalline ices than for the amorphous samples.

The high explained variance of the 1st principal component of the set consisting of water spectra demonstrates that the energy bins of the water spectra are highly correlated with each other in such a way that the spectral changes are

TABLE II. Scores of the 1st loading for the various water spectra and their predicted temperatures from linear regression using a single-principal-component model. The loading of the 1st principal component from the set of water spectra is shown in Fig. 5 (double-dotted red curve).

Spectrum	Score	Predicted temperature (K)
H ₂ O 299 K	0.049	294
H ₂ O 280 K	0.001	278
H ₂ O 270 K	-0.010	276
H ₂ O 264 K	-0.040	258

TABLE III. Scores of the 1st loading for the various water and ice spectra. The loading of the 1st principal component from the set of water and ice spectra is shown in Fig. 5 (solid black curve).

Spectrum	Score
H ₂ O/Si ₃ N ₄ 299 K	0.136
H ₂ O/Si ₃ N ₄ 280 K	0.109
H ₂ O/Si ₃ N ₄ 270 K	0.010
H ₂ O/Si ₃ N ₄ 264 K	0.081
H ₂ O/Si ₃ N ₄ 232 K	-0.104
D ₂ O/Pt(111) 100 K	-0.027
D ₂ O/Pt(111) 150 K	-0.131
D ₂ O/BaF ₂ (111) 144 K	-0.165

described almost entirely by the loading of the 1st principal component. This means that the difference spectra in Fig. 1 all have similar shape to the loading of the 1st principal component, so that the difference spectra can be reproduced by the loading of the 1st principal component scaled by a scalar value, namely, the score of each spectrum (in the current analysis, the scores of the spectra will reproduce the difference spectra with respect to the mean of all spectra, but similar scores could be calculated that reproduce the difference spectra with respect to the spectrum measured at 299 K). When both water and ice spectra are included in the principal component analysis, the explained variance of the 1st principal component is reduced notably and the resemblance between the difference spectra and the loading of the 1st principal component is weakened.

IV. DISCUSSION

The temperature dependence of the O K-edge x-ray absorption spectra of water supports that tetrahedral ordering is increasing in the liquid upon cooling below room temperature; similar trends have been observed previously using x-ray scattering,^{40,92,93} infrared spectroscopy,^{44,77,94–96} and x-ray emission spectroscopy.^{9,43,97} The principal component analysis shows that a single principal component is sufficient to describe the changes in the liquid spectrum with temperature, which is consistent with the hypothesis that water structure can be viewed in terms of fluctuations around two structural motifs where the pre-edge and most of the main-edge intensity are related to HDL species and the post-edge mainly to LDL species.^{9,17} We note that conversion between two species is also consistent with the existence of an isosbestic point in the otherwise featureless Raman OH stretch spectra of HDO in water although an isosbestic point alone is not proof, since also a single-component system can exhibit an isosbestic point.⁹⁸ The ability of a linear model based on a single principal component to describe the observed changes suggests that the conversion between HDL and LDL species would to first order be linear with temperature in the regime where the liquid was studied. This hypothesis can be extended to all amorphous spectra, where we mostly see relative changes in amplitude of the various peaks and the 1st principal component therefore still explains nearly all sample variance (96%). However, the variations of the spectra are

no longer linear with temperature, since the single principal component model in this case only explains 39% of the sample temperature variation. When including crystalline samples, the addition of a more complex spectral distribution in the post-edge region lowers the efficiency of the 1st principal component, and the spectral changes can no longer be described as a conversion between HDL and LDL species. We assign these changes in the crystal phase to long-range band-structure effects that appear from critical points in the Brillouin zone, see discussion below.

An alternative interpretation of the pre-edge is that it is due to a localized core excitation, a so-called core-exciton, in a tetrahedrally H-bonded network with only minor distortions.^{20,28} Based on a van't Hoff analysis of the temperature dependence of the pre-edge intensity, an energy difference between species associated with the pre-edge and the rest of the liquid was estimated at around 0.9 kcal/mol and, based on such a small energy difference, only minor distortions from a tetrahedral network were concluded.²⁰ That this conclusion is incorrect is clear since the enthalpy difference between low-density amorphous (LDA) and high-density amorphous (HDA) ice has been measured to 0.18 ± 0.04 kcal/mol⁹⁹ at 1 atm in spite of the large difference in local structure¹⁰⁰ and resulting density. The problem with this conclusion on structural changes is that it neglects the fact that stabilizing interactions depend on structure in an H-bonding liquid such as water; in tetrahedral structures the local density is low, which reduces the importance of the van der Waals attraction, while in disordered, close-packed structures the van der Waals attraction becomes more important as the local density increases through loss of directional H-bonds.^{101–103} Indeed, based on various theoretical methods^{41,101} it has recently been shown that even large variations in local structures in simulated water can result in small energy differences. Furthermore, the entropy is lower in tetrahedral structures, since in that case the quantized librational modes are not accessible thermally and do not contribute to the entropy, while for disordered structures they do.^{17,42} Using the results of a van't Hoff analysis to quantify the extent of structural changes in neat liquid water without taking these effects into account is thus not possible.

A van't Hoff analysis of spectroscopic data is furthermore intrinsically binary, although the spectroscopic response within the assumed two classes is the average of the response of many different structural variations within each class. To compound matters further, there are longer range interactions in water through, e.g., many-body effects and H-bond cooperativity,¹⁰⁴ leading to different structural length scales that vary with temperature which are detected differently depending on the applied spectroscopy.^{9,17,105} Since different spectroscopies show different sensitivity to different substructures it is clear that a van't Hoff analysis of temperature-dependent spectral features can give large differences depending on the applied spectroscopy.^{9,20,27,106–109} That the conclusion of only minor distortions is problematic has also been demonstrated experimentally through recent vibrationally resolved O K-edge RIXS data, where an OH-stretch frequency close to gas phase has been found for molecules contributing significantly to the pre-edge intensity.⁷⁰

If the pre-edge peak is associated with weak or broken H-bonds, what is the reason that we still see it in ice? If we disregard the isotope effect giving a slightly higher pre-edge peak for H₂O in comparison to D₂O^{1,15} we can make a comparison between the different systems in Table I. We note that only a fraction of the pre-edge intensity from water at 299 K remains in the ice samples, with 48% for H₂O ice at 232 K on Si₃N₄, 60% for D₂O amorphous ice at 100 K on Pt(111), 50% for D₂O crystalline ice at 150 K on Pt(111), but only 18% for D₂O ice on BaF₂ at 144 K. If we add also the previous XRS study where it was claimed that the change in pre-edge intensity between water and ice is rather small, with a remaining pre-edge intensity of the order 70% in bulk hexagonal ice,²⁰ there is quite a variation. There seems not to be a simple estimation of the pre-edge intensity in hexagonal or cubic ice. In fact, with D₂O ice on BaF₂ we now have a sample that has a small pre-edge intensity of the order of a factor 5 less than in water. This would be consistent with the above notion that indeed the pre-edge is related to severely distorted H-bonds.

Here we present a hypothesis that could explain the variation in the pre-edge of the different ice spectra as due to varying degrees of admixture of HDA ice.¹⁵ It has been established that both the pre-edge and main-edge are increased for HDA ice as measured by XRS.²⁸ A contribution of HDA ice will therefore significantly increase the pre-edge intensity. Indeed an extended x-ray absorption fine structure (EXAFS) study of crystalline ice grown on Au(111) showed that the film, when measured, was not a pure phase but a mixture of hexagonal and HDA ice.^{110,111} In fact, even if the ice were prepared as a pure hexagonal ice phase the interaction with the beam can be expected to transform portions of the ice to HDA ice. We know that the enthalpy difference between ice I_h and HDA ice is 0.58 ± 0.1 kcal/mol⁹⁹ at 1 atm while the absorption of a photon at 535 eV corresponds to 12340 kcal/mol, which is 4 orders of magnitude higher and thus sufficient to convert ice I_h into HDA ice if the energy is not effectively transferred away from the excited molecule. We can anticipate that the absorbed energy will dissipate slowly through the solid creating many sites where significant energy is dumped causing a pressure effect that converts a fraction of the volume into HDA ice. Since the temperature is low, most molecules are kinetically hindered to convert back to normal hexagonal ice. In the liquid state, on the other hand, the higher mobility and ultrafast dynamics of breaking and forming H-bonds on picosecond timescales¹¹² allows a beam-induced structural defect to convert back nearly immediately and no beam-induced transformation will be seen, except perhaps upon extreme supercooling.

It is often assumed that XRS, since it has much larger penetration depth, should disturb a sample much less compared to soft XAS. However, due to the extremely small cross-section for the inelastic x-ray Raman excitation an extremely high photon flux is often required in order to measure a spectrum resulting in that the overall energy density deposited in the sample might be similar in XRS and XAS measurements. This is different from x-ray diffraction studies since the elastic scattering cross-section is much higher and less photon flux is required. We propose further that there is a higher probability for this beam-induced transformation close to grain bound-

aries. This could be the reason for the smaller pre-edge intensity for ice on BaF₂(111) in comparison to on Pt(111) since the low defect density on BaF₂ gives few nucleation sites and larger crystallites. Note, however, the small contribution at 533 eV from radiation-induced OH at the BaF₂ surface which may provide nucleation sites affecting the long-range order in the crystallites.

In the case of monolayer water on metal surfaces the pre-edge is nearly missing¹⁵ which, within this hypothesis, can be understood in terms of the metal surface very efficiently taking up the energy deposited by the high-energy electrons, where furthermore a large fraction of the electrons is emitted into vacuum. That ice on BaF₂ seems to be more crystalline is indicated by the enhanced intensity in the multiple-scattering resonances above the post-edge. These are connected to critical points in the long-range band structure where the bands disperse less giving rise to associated features in the density of states. As some HDA ice is incorporated into the lattice it will destroy the long-range order resulting in a diminishing of the multiple-scattering resonance intensities. We therefore expect that the spectrum of ice prepared on BaF₂ with a significantly smaller pre-edge and strong multiple-scattering resonances better reflects an unperturbed ice spectrum of hexagonal or cubic ice than the other measured ice spectra. This indeed means that there is a large difference in pre-edge intensity between water and ice. Here we propose that in unperturbed ice there is only an extremely weak pre-edge where the small intensity is due to vibronic coupling to asymmetric molecular vibrations that break the instantaneous near-tetrahedral symmetry.^{7,15}

V. CONCLUSIONS

We conclude that the increased tetrahedral ordering in the H-bonded network in liquid water upon cooling is reflected through a decrease in pre-edge absorption cross-section and an increased post-edge resonance when probed by XAS. This is modeled accurately by a single principal component, which through linear regression can predict the sample temperature to sufficient (± 6 K) level. Similar observations extend to amorphous water at lower temperatures, but in this temperature regime the spectral variations are no longer linear with temperature.

Crystalline ice films are governed by growth conditions that strongly affect the defect density and the grain size. Although crystalline ice films all exhibit a split of the post-edge into two peaks, the absorption cross-section at the pre-edge—associated with asymmetrically H-bonded SD species—varies strongly. We demonstrate that ice grown on BaF₂(111) can result in a reduced pre-edge to the extent that it is almost negligible. Additionally, an increase in absorption cross-section between 544 and 548 eV suggests a notable extension of the H-bonded network in the case of ice grown on BaF₂ as compared to other growth conditions, with well-resolved high-symmetry points in the electronic band-structure at higher energies. This can be understood in terms of the Newns-Anderson impurity model applied to XAS of water and ice, in which the core-excited atomic orbitals hybridize with the conduction band of the surrounding

H-bonding network to create the spectral features.¹⁷ The reduced absorption cross-section at the pre-edge and main-edge indicates stronger hybridization, which shifts the delocalized post-edge resonance to higher energy and results in the observed increase in absorption cross-section between 544 and 548 eV.

ACKNOWLEDGMENTS

This work was supported by the Swedish Research Council and the Department of Energy through the SLAC Laboratory Directed Research and Development Program. The measurements were carried out at the Stanford Synchrotron Radiation Lightsource (SSRL) and the Advanced Light Source (ALS), both national user facilities operated by Stanford University and U.C. Berkeley, respectively, on behalf of the U.S. Department of Energy, Office of Basic Energy Sciences. The ALS and the MES beamline 11.0.2 are supported by the Director, Office of Science, Office of Basic Energy Sciences, Division of Chemical Sciences, Geosciences and Biosciences and Materials Sciences Division of the U.S. Department of Energy at the Lawrence Berkeley National Laboratory under Contract No. DE-AC02-05CH11231.

- ¹U. Bergmann *et al.*, "Isotope effects in liquid water probed by x-ray Raman spectroscopy," *Phys. Rev. B* **76**, 024202 (2007).
- ²U. Bergmann *et al.*, "X-ray Raman spectroscopy at the oxygen K edge of water and ice: Implications on local structure models," *Phys. Rev. B* **66**, 092107 (2002).
- ³C. D. Cappa, J. D. Smith, B. M. Messer, R. C. Cohen, and R. J. Saykally, "Effects of cations on the hydrogen bond network of liquid water: New results from X-ray absorption spectroscopy of liquid microjets," *J. Phys. Chem. B* **110**, 5301–5309 (2006).
- ⁴C. D. Cappa, J. D. Smith, B. M. Messer, R. C. Cohen, and R. J. Saykally, "Nature of the aqueous hydroxide ion probed by X-ray absorption spectroscopy," *J. Phys. Chem. A* **111**, 4776–4785 (2007).
- ⁵C. D. Cappa *et al.*, "Effects of alkali metal halide salts on the hydrogen bond network of liquid water," *J. Phys. Chem. B* **109**, 7046–7052 (2005).
- ⁶M. Cavalleri *et al.*, "The local structure of protonated water from X-ray absorption and density functional theory," *J. Chem. Phys.* **124**, 194508 (2006).
- ⁷M. Cavalleri, H. Ogasawara, L. G. M. Pettersson, and A. Nilsson, "The interpretation of X-ray absorption spectra of water and ice," *Chem. Phys. Lett.* **364**, 363–370 (2002).
- ⁸C. Chen *et al.*, "Solvation structures of protons and hydroxide ions in water," *J. Chem. Phys.* **138**, 154506 (2013).
- ⁹C. Huang *et al.*, "The inhomogeneous structure of water at ambient conditions," *Proc. Natl. Acad. Sci. U.S.A.* **106**, 15214–15218 (2009).
- ¹⁰N. Huang *et al.*, "Microscopic probing of the size dependence in hydrophobic solvation," *J. Chem. Phys.* **136**, 074507 (2012).
- ¹¹S. Kaya *et al.*, "Highly compressed two-dimensional form of water at ambient conditions," *Sci. Rep.* **3**, 1074 (2013).
- ¹²S. Myneni *et al.*, "Spectroscopic probing of local hydrogen-bonding structures in liquid water," *J. Phys.: Condens. Matter* **14**, L213–L219 (2002).
- ¹³L. Å. Näslund *et al.*, "X-ray absorption spectroscopy study of the hydrogen bond network in the bulk water of aqueous solutions," *J. Phys. Chem. A* **109**, 5995 (2005).
- ¹⁴L. Å. Näslund *et al.*, "X-ray absorption spectroscopy measurements of liquid water," *J. Phys. Chem. B* **109**, 13835 (2005).
- ¹⁵A. Nilsson *et al.*, "X-ray absorption spectroscopy and x-ray Raman scattering of water and ice: An experimental view," *J. Electron Spectrosc. Relat. Phenom.* **177**, 99–129 (2010).
- ¹⁶A. Nilsson *et al.*, "The hydrogen bond in ice probed by soft x-ray spectroscopy and density functional theory," *J. Chem. Phys.* **122**, 154505 (2005).
- ¹⁷A. Nilsson and L. G. M. Pettersson, "Perspective on the structure of liquid water," *Chem. Phys.* **389**, 1–34 (2011).
- ¹⁸H. Ogasawara *et al.*, "Structure and bonding of water on Pt(111)," *Phys. Rev. Lett.* **89**, 276102 (2002).
- ¹⁹T. Pykkänen *et al.*, "Role of non-hydrogen-bonded molecules in the oxygen K-edge spectrum in ice," *J. Phys. Chem. B* **114**, 3804 (2010).
- ²⁰T. Pykkänen *et al.*, "Temperature dependence of the near-edge spectrum of water," *J. Phys. Chem. B* **115**, 14544–14550 (2011).
- ²¹C. J. Sahle *et al.*, "Microscopic structure of water at elevated pressures and temperatures," *Proc. Natl. Acad. Sci. U.S.A.* **110**, 6301–6306 (2013).
- ²²T. Schiros, K. J. Andersson, L. G. M. Pettersson, A. Nilsson, and H. Ogasawara, "Chemical bonding of water to metal surfaces studied with core-level spectroscopies," *J. Electron Spectrosc. Relat. Phenom.* **177**, 85–98 (2010).
- ²³T. Schiros *et al.*, "Structure and bonding of water-hydroxyl mixed phase on Pt(111)," *J. Phys. Chem. C* **111**, 15003–15012 (2007).
- ²⁴T. Schiros *et al.*, "Structure of water adsorbed on Cu(110): H-up, H-down, or both?," *Chem. Phys. Lett.* **429**, 415 (2006).
- ²⁵T. Schiros *et al.*, "The role of substrate electrons in the wetting of a metal surface," *J. Chem. Phys.* **132**, 094701 (2010).
- ²⁶J. D. Smith *et al.*, "Probing the local structure of liquid water by x-ray absorption spectroscopy," *J. Phys. Chem. B* **110**, 20038–20045 (2006).
- ²⁷J. D. Smith *et al.*, "Energetics of hydrogen bond rearrangements in liquid water," *Science* **306**, 851 (2004).
- ²⁸J. S. Tse *et al.*, "X-ray Raman spectroscopic study of water in the condensed phases," *Phys. Rev. Lett.* **100**, 095502 (2008).
- ²⁹I. Waluyo *et al.*, "The structure of water in the hydration shell of cations from x-ray Raman and small angle x-ray scattering measurements," *J. Chem. Phys.* **134**, 064513 (2011).
- ³⁰I. Waluyo *et al.*, "Increased fraction of low-density structures in aqueous solutions of fluoride," *J. Chem. Phys.* **134**, 224507 (2011).
- ³¹I. Waluyo, D. Nordlund, U. Bergmann, L. G. M. Pettersson, and A. Nilsson, "Increased fraction of weakened hydrogen bonds of water in AOT reverse micelles," *J. Chem. Phys.* **131**, 031103 (2009).
- ³²P. Wernet, "Electronic structure in real time: Mapping valence electron rearrangements during chemical reactions," *Phys. Chem. Chem. Phys.* **13**, 16941–16954 (2011).
- ³³P. Wernet *et al.*, "The structure of the first coordination shell in liquid water," *Science* **304**, 995–999 (2004).
- ³⁴P. Wernet *et al.*, "Spectroscopic characterization of microscopic hydrogen bonding disparities in supercritical water," *J. Chem. Phys.* **123**, 154503 (2005).
- ³⁵D. T. Bowron *et al.*, "X-ray-Raman scattering from the oxygen K edge in liquid and solid H₂O," *Phys. Rev. B* **62**, R9223–R9227 (2000).
- ³⁶N. Huang *et al.*, "X-ray Raman scattering provides evidence for interfacial acetonitrile-water dipole interactions in aqueous solutions," *J. Chem. Phys.* **135**, 164509 (2011).
- ³⁷K. M. Lange *et al.*, "On the origin of the hydrogen-bond-network nature of water: X-ray absorption and emission spectra of water-acetonitrile mixtures," *Angew. Chem.* **123**, 1–6 (2011).
- ³⁸N. Huse *et al.*, "Probing the hydrogen-bond network of water via time-resolved soft x-ray spectroscopy," *Phys. Chem. Chem. Phys.* **11**, 3951 (2009).
- ³⁹P. Parent, C. Laffon, C. Mangeney, F. Bournel, and M. Tronc, "Structure of the water ice surface studied by x-ray absorption spectroscopy at the O K-edge," *J. Chem. Phys.* **117**, 10842–10851 (2002).
- ⁴⁰C. Huang *et al.*, "Wide-angle x-ray diffraction and molecular dynamics study of medium-range order in ambient and hot water," *Phys. Chem. Chem. Phys.* **13**, 19997–20007 (2011).
- ⁴¹M. Leetmaa *et al.*, "Diffraction and IR/Raman data do not prove tetrahedral water," *J. Chem. Phys.* **129**, 084502 (2008).
- ⁴²A. Nilsson, C. Huang, and L. G. M. Pettersson, "Fluctuations in ambient water," *J. Mol. Liq.* **176**, 2–16 (2012).
- ⁴³T. Tokushima *et al.*, "High resolution x-ray emission spectroscopy of liquid water: The observation of two structural motifs," *Chem. Phys. Lett.* **460**, 387–400 (2008).
- ⁴⁴A. Taschin, P. Bartolini, R. Eramo, R. Righini, and R. Torre, "Evidence of two distinct local structures of water from ambient to supercooled conditions," *Nat. Commun.* **4**, 2401 (2013).
- ⁴⁵G. N. I. Clark, C. D. Cappa, J. D. Smith, R. J. Saykally, and T. Head-Gordon, "The structure of ambient water," *Mol. Phys.* **108**, 1415–1433 (2010).
- ⁴⁶A. K. Soper, "Recent water myths," *Pure Appl. Chem.* **82**, 1855 (2010).
- ⁴⁷A. K. Soper, J. Teixeira, and T. Head-Gordon, "Is ambient water inhomogeneous on the nanometer-length scale?," *Proc. Natl. Acad. Sci. U.S.A.* **107**, E44 (2010).

- ⁴⁸C. Huang *et al.*, "Reply to Soper *et al.*, "Fluctuations in water around a bimodal distribution of local hydrogen bonded structural motifs";" *Proc. Natl. Acad. Sci. U.S.A.* **107**, E45 (2010).
- ⁴⁹A. Nilsson *et al.*, "Comment on "Energetics of hydrogen bond network rearrangements in liquid water,"" *Science* **308**, 793a (2005).
- ⁵⁰J. D. Smith, C. D. Cappa, B. M. Messer, R. C. Cohen, and R. J. Saykally, "Response to comment on energetics of hydrogen bond network rearrangements in liquid water," *Science* **308**, 793b (2005).
- ⁵¹J. D. Smith *et al.*, "Unified description of temperature-dependent hydrogen-bond rearrangements in liquid water," *Proc. Natl. Acad. Sci. U.S.A.* **102**, 14171 (2005).
- ⁵²P. H. Poole, F. Sciortino, U. Essmann, and H. E. Stanley, "Phase-behavior of metastable water," *Nature (London)* **360**, 324–328 (1992).
- ⁵³D. T. Limmer and D. Chandler, "The putative liquid-liquid transition is a liquid-solid transition in atomistic models of water," *J. Chem. Phys.* **135**, 134503 (2011).
- ⁵⁴D. Nordlund *et al.*, "Sensitivity of X-ray absorption spectroscopy to hydrogen bond topology," *Phys. Rev. B* **80**, 233404 (2009).
- ⁵⁵D. Nordlund *et al.*, "Attosecond timescale probing of electron delocalization in liquid water and ice," *Phys. Rev. Lett.* **99**, 217406 (2007).
- ⁵⁶L. Triguero, L. G. M. Pettersson, and H. Ågren, "Calculations of near-edge x-ray absorption spectra of gas phase and chemisorbed molecules by means of density functional and transition potential theory," *Phys. Rev. B* **58**, 8097 (1998).
- ⁵⁷M. Leetmaa, M. P. Ljungberg, A. P. Lyubartsev, A. Nilsson, and L. G. M. Pettersson, "Theoretical approximations to x-ray absorption spectroscopy of liquid water and ice," *J. Electron Spectrosc. Relat. Phenom.* **177**, 135–157 (2010).
- ⁵⁸R. G. Wilks, J. B. MacNaughton, H.-B. Kraatz, T. Regier, and A. Moewes, "Combined x-ray absorption spectroscopy and density functional theory examination of ferrocene-labeled peptides," *J. Phys. Chem. B* **110**, 5955–5965 (2006).
- ⁵⁹C. Kolczewski, K. Hermann, S. Guimond, H. Kuhlenbeck, and H.-J. Freund, "Identification of the vanadyl terminated $V_2O_3(0001)$ surface by means of O K-edge NEXAFS: A combined theoretical and experimental study," *Surf. Sci.* **601**, 5394 (2007).
- ⁶⁰E. F. Aziz, M. Freiwald, S. Eisebitt, and W. Eberhardt, "Steric hindrance of ion-ion interaction in electrolytes," *Phys. Rev. B* **73**, 075120 (2006).
- ⁶¹C. Kolczewski *et al.*, "Detailed study of pyridine at the C 1s and N 1s ionization thresholds: The influence of the vibrational fine structure," *J. Chem. Phys.* **115**, 6426–6437 (2001).
- ⁶²M. Odellius, M. Cavalleri, A. Nilsson, and L. G. M. Pettersson, "The X-ray absorption spectrum of liquid water from molecular dynamics simulations: Asymmetric model," *Phys. Rev. B* **73**, 024205 (2006).
- ⁶³D. Prendergast and G. Galli, "X-ray absorption spectra of water from first principles calculations," *Phys. Rev. Lett.* **96**, 215502 (2006).
- ⁶⁴B. Hetényi, F. De Angelis, P. Giannozzi, and R. Car, "Calculation of near-edge x-ray-absorption fine structure at finite temperatures: Spectral signatures of hydrogen bond breaking in liquid water," *J. Chem. Phys.* **120**, 8632–8637 (2004).
- ⁶⁵M. Cavalleri, M. Odellius, D. Nordlund, A. Nilsson, and L. G. M. Pettersson, "Half or full core hole in density functional theory X-ray absorption spectrum calculations of water?," *Phys. Chem. Chem. Phys.* **7**, 2854–2858 (2005).
- ⁶⁶W. Chen, X. Wu, and R. Car, "X-ray absorption signatures of the molecular environment in water and ice," *Phys. Rev. Lett.* **105**, 017802 (2010).
- ⁶⁷L. Kong, X. Wu, and R. Car, "Roles of quantum nuclei and inhomogeneous screening in the x-ray absorption spectra of water and ice," *Phys. Rev. B* **86**, 134203 (2012).
- ⁶⁸J. Vinson, J. J. Kas, J. J. Rehr, F. D. Vila, and E. L. Shirley, "Theoretical optical and x-ray spectra of liquid and solid H_2O ," *Phys. Rev. B* **85**, 045101 (2012).
- ⁶⁹M. Iannuzzi, "X-ray absorption spectra of hexagonal ice and liquid water by all-electron Gaussian and augmented plane wave calculations," *J. Chem. Phys.* **128**, 204506 (2008).
- ⁷⁰Y. Harada *et al.*, "Selective probing of the OH or OD stretch vibration in liquid water using resonant inelastic soft-x-ray scattering," *Phys. Rev. Lett.* **111**, 193001 (2013).
- ⁷¹A. L. D. Kilcoyne *et al.*, "Interferometer-controlled scanning transmission X-ray microscopes at the advanced light source," *J. Synchrotron Radiat.* **10**, 125–136 (2003).
- ⁷²A. Savitzky and M. J. E. Golay, "Smoothing and differentiation of data by simplified least squares procedures," *Anal. Chem.* **36**, 1627–1639 (1964).
- ⁷³K. L. Pearson III, "On lines and planes of closest fit to systems of points in space," *Philos. Mag. Ser. 6* **2**, 559–572 (1901).
- ⁷⁴H. Hotelling, "Analysis of a complex of statistical variables into principal components," *J. Educ. Psychol.* **24**, 417–441 (1933).
- ⁷⁵H. Hotelling, "Analysis of a complex of statistical variables into principal components," *J. Educ. Psychol.* **24**, 498–520 (1933).
- ⁷⁶H. Abdi and L. J. Williams, "Principal component analysis," *Wiley Interdiscip. Rev.: Comput. Stat.* **2**, 433–459 (2010).
- ⁷⁷V. H. Segtnan, Š. Šašić, T. Isaksson, and Y. Ozaki, "Studies on the structure of water using two-dimensional near-infrared correlation spectroscopy and principal component analysis," *Anal. Chem.* **73**, 3153–3161 (2001).
- ⁷⁸Y. He, X. Li, and X. Deng, "Discrimination of varieties of tea using near infrared spectroscopy by principal component analysis and BP model," *J. Food Eng.* **79**, 1238–1242 (2007).
- ⁷⁹A. C. Scheinost, R. Kretzschmar, S. Pfister, and D. R. Roberts, "Combining selective sequential extractions, x-ray absorption spectroscopy, and principal component analysis for quantitative zinc speciation in soil," *Environ. Sci. Technol.* **36**, 5021–5028 (2002).
- ⁸⁰Y. H. Choi *et al.*, "Metabolomic differentiation of cannabis sativa cultivars using 1H NMR spectroscopy and principal component analysis," *J. Nat. Prod.* **67**, 953–957 (2004).
- ⁸¹K. Amann-Winkel *et al.*, "Water's second glass transition," *Proc. Natl. Acad. Sci. U.S.A.* **110**, 17720–17725 (2013).
- ⁸²G. P. Johari, A. Hallbrucker, and E. Mayer, "The glass-liquid transition of hyperquenched water," *Nature (London)* **330**, 552–553 (1987).
- ⁸³J. A. McMillan and S. C. Los, "Vitreous ice: Irreversible transformations during warm-up," *Nature* **206**, 806–807 (1965).
- ⁸⁴M. S. Elsaesser, K. Winkel, E. Mayer, and T. Loerting, "Reversibility and isotope effect of the calorimetric glass \rightarrow liquid transition of low-density amorphous ice," *Phys. Chem. Chem. Phys.* **12**, 708–712 (2010).
- ⁸⁵M. A. Henderson, "Water on surface review," *Surf. Sci. Rep.* **46**, 1 (2002).
- ⁸⁶Z. Dohnálek *et al.*, "Substrate induced crystallization of amorphous solid water at low temperatures," *J. Chem. Phys.* **110**, 5489–5492 (1999).
- ⁸⁷G. A. Kimmel, N. G. Petrik, Z. Dohnálek, and B. D. Kay, "Crystalline ice growth on Pt(111): Observation of a hydrophobic water monolayer," *Phys. Rev. Lett.* **95**, 166102 (2005).
- ⁸⁸G. A. Kimmel, N. G. Petrik, Z. Dohnálek, and B. D. Kay, "Crystalline ice growth on Pt(111) and Pd(111): Nonwetting growth on a hydrophobic water monolayer," *J. Chem. Phys.* **126**, 114702 (2007).
- ⁸⁹P. Löfgren, P. Ahlström, D. V. Chakarov, J. Lausmaa, and B. Kasemo, "Substrate dependent sublimation kinetics of mesoscopic ice films," *Surf. Sci.* **367**, L19–L25 (1996).
- ⁹⁰P. Löfgren, P. Ahlström, J. Lausmaa, B. Kasemo, and D. Chakarov, "Crystallization kinetics of thin amorphous water films on surfaces," *Langmuir* **19**, 265–274 (2003).
- ⁹¹I. Waluyo *et al.*, "Spectroscopic evidence for the formation of 3-D crystallites during isothermal heating of amorphous ice on Pt(111)," *Surf. Sci.* **602**, 2004 (2008).
- ⁹²J. Neufeind, C. J. Benmore, J. K. R. Weber, and D. Paschek, "More accurate X-ray scattering data of deeply supercooled bulk liquid water," *Mol. Phys.* **109**, 279–288 (2011).
- ⁹³J. A. Sellberg *et al.*, "Ultrafast X-ray probing of water structure below the homogeneous ice nucleation temperature," *Nature* **510**, 381–384 (2014).
- ⁹⁴Y. Maréchal, "The molecular structure of liquid water delivered by absorption spectroscopy in the whole IR region completed with thermodynamics data," *J. Mol. Struct.* **1004**, 146–155 (2011).
- ⁹⁵Q. Sun, "Local statistical interpretation for water structure," *Chem. Phys. Lett.* **568–569**, 90–94 (2013).
- ⁹⁶L. Xu *et al.*, "Appearance of a fractional Stokes-Einstein relation in water and a structural interpretation of its onset," *Nat. Phys.* **5**, 565–569 (2009).
- ⁹⁷T. Tokushima *et al.*, "High resolution X-ray emission spectroscopy of water and its assignment based on two structural motifs," *J. Electron Spectrosc. Relat. Phenom.* **177**, 192–205 (2010).
- ⁹⁸P. L. Geissler, "Temperature dependence of inhomogeneous broadening: On the meaning of isosbestic points," *J. Am. Chem. Soc.* **127**, 14930–14935 (2005).
- ⁹⁹O. Mishima, L. D. Calvert, and E. Whalley, "'Melting ice' I at 77 K and 10 kbar: A new method of making amorphous solids," *Nature (London)* **310**, 393–395 (1984).
- ¹⁰⁰D. T. Bowron *et al.*, "The local and intermediate range structures of the five amorphous ices at 80 K and ambient pressure: A Faber-Ziman and Bhatia-Thornton analysis," *J. Chem. Phys.* **125**, 194502 (2006).

- ¹⁰¹A. Møgelhøj *et al.*, “Ab initio van der Waals interactions in simulations of water alter structure from mainly tetrahedral to high-density-like,” *J. Phys. Chem. B* **115**, 14149–14160 (2011).
- ¹⁰²F. Corsetti, E. Artacho, J. M. Soler, S. S. Alexandre, and M.-V. Fernandez-Serra, “Room temperature compressibility and diffusivity of liquid water from first principles,” *J. Chem. Phys.* **139**, 194502 (2013).
- ¹⁰³B. Santra *et al.*, “Hydrogen bonds and van der Waals forces in ice at ambient and high pressure,” *Phys. Rev. Lett.* **107**, 185701 (2011).
- ¹⁰⁴L. Ojamäe and K. Hermansson, “An ab initio study of cooperativity in water chains: Interaction energies and anharmonic frequencies,” *J. Phys. Chem.* **98**, 4271 (1994).
- ¹⁰⁵C. Huang *et al.*, “Increasing correlation length in bulk supercooled H₂O, D₂O, and NaCl solution determined from small angle x-ray scattering,” *J. Chem. Phys.* **133**, 134504 (2010).
- ¹⁰⁶G. E. Walrafen, “Effects of equilibrium H-bond distance and angle changes on Raman intensities from water,” *J. Chem. Phys.* **120**, 4868–4876 (2004).
- ¹⁰⁷G. E. Walrafen, “Raman H-bond pair volume for water,” *J. Chem. Phys.* **121**, 2729–2736 (2004).
- ¹⁰⁸G. E. Walrafen, M. R. Fisher, M. S. Hokmabadi, and W.-H. Yang, “Temperature dependence of the low- and high-frequency Raman scattering from liquid water,” *J. Chem. Phys.* **85**, 6970–6982 (1986).
- ¹⁰⁹G. E. Walrafen, M. S., Hokmabadi, and W.-H. Yang, “Raman isosbestic points from liquid water,” *J. Chem. Phys.* **85**, 6964–6969 (1986).
- ¹¹⁰Y. Zubavichus *et al.*, “Local structure of amorphous ice as revealed by O K-edge EXAFS,” *ChemPhysChem* **5**, 509–514 (2004).
- ¹¹¹Y. Zubavichus *et al.*, “Oxygen K-edge X-ray absorption fine structure studies of vacuum-deposited ice films,” *Langmuir* **22**, 7241–7247 (2006).
- ¹¹²E. T. J. Nibbering and T. Elsaesser, “Ultrafast vibrational dynamics of hydrogen bonds in the condensed phase,” *Chem. Rev.* **104**, 1887–1914 (2004).